Track structure of protons and other light ions in liquid water: Applications of the LIonTrack code at the nanometer scale

G. Bäckström
Department of Radiology, Oncology and Radiation Science, Section of Medical Radiation Physics, Uppsala University, Akademiska Sjukhuset, SE-751 85 Uppsala, Sweden

M. E. Galassi
Instituto de Física de Rosario, CONICET-UNR, Av. Pellegrini 250, 2000 Rosario, Argentina

N. Tilly
Department of Radiology, Oncology and Radiation Science, Section of Medical Radiation Physics, Uppsala University, Akademiska Sjukhuset, SE-751 85 Uppsala, Sweden and Elekta Instrument AB, Box 1704, 75147 Uppsala, Sweden

A. Ahnesjö
Department of Radiology, Oncology and Radiation Science, Section of Medical Radiation Physics, Uppsala University, Akademiska Sjukhuset, SE-751 85 Uppsala, Sweden

J. M. Fernández-Varea[a)]
Facultat de Física (ECM and ICC), Universitat de Barcelona, Diagonal 645, E-08028 Barcelona, Spain

(Received 21 November 2012; revised 12 April 2013; accepted for publication 12 April 2013; published 10 May 2013)

Purpose: The LIonTrack (Light Ion Track) Monte Carlo (MC) code for the simulation of H^+, He^{2+}, and other light ions in liquid water is presented together with the results of a novel investigation of energy-deposition site properties from single ion tracks.
Methods: The continuum distorted-wave formalism with the eikonal initial state approximation (CDW-EIS) is employed to generate the initial energy and angle of the electrons emitted in ionizing collisions of the ions with H_2O molecules. The model of Dingfelder *et al.* ["Electron inelastic-scattering cross sections in liquid water," Radiat. Phys. Chem. **53**, 1–18 (1998); "Comparisons of calculations with PARTRAC and NOREC: Transport of electrons in liquid water," Radiat. Res. **169**, 584–594 (2008)] is linked to the general-purpose MC code PENELOPE/penEasy to simulate the inelastic interactions of the secondary electrons in liquid water. In this way, the extended PENELOPE/penEasy code may provide an improved description of the 3D distribution of energy deposits (EDs), making it suitable for applications at the micrometer and nanometer scales.
Results: Single-ionization cross sections calculated with the *ab initio* CDW-EIS formalism are compared to available experimental values, some of them reported very recently, and the theoretical electronic stopping powers are benchmarked against those recommended by the ICRU. The authors also analyze distinct aspects of the spatial patterns of EDs, such as the frequency of nearest-neighbor distances for various radiation qualities, and the variation of the mean specific energy imparted in nanoscopic targets located around the track. For 1 MeV/u particles, the C^{6+} ions generate about 15 times more clusters of six EDs within an ED distance of 3 nm than H^+.
Conclusions: On average clusters of two to three EDs for 1 MeV/u H^+ and clusters of four to five EDs for 1 MeV/u C^{6+} could be expected for a modeling double strand break distance of 3.4 nm.
 [http://dx.doi.org/10.1118/1.4803464]

Key words: track structure of protons and light ions, spatial patterns of energy deposits, Monte Carlo code, CDW-EIS model

I. INTRODUCTION

To get a better insight into the variation of the relative biological effectiveness (RBE) with radiation quality, it is desirable to make a detailed analysis of the distinct spatial patterns of energy deposits (EDs) (Ref. 3) at the nanometer scale.[4,5] To date, such data are not available from experiments done in liquid water, but certain quantities like ionization-cluster-size distributions at the nanometer scale have been measured in gas-filled proportional counters and correlated to liquid water.[5] Another approach to study the patterns of EDs is to utilize track-structure Monte Carlo (MC) codes[6–9] to carry out detailed, i.e., event-by-event, simulation in liquid water.

In the last few decades, several MC codes have been developed within the ambit of micro-dosimetry, see the review article by Nikjoo *et al.*[10] Some of these are devoted to the transport of electrons, e.g., DELTA,[11] KURBUC,[12] and NOREC,[13] while others simulate the passage of protons and other light ions, e.g., PITS04,[14] MC4,[7] PARTRAC,[15] RITRACKS,[16] as well as the codes developed by Champion *et al.*,[8] Wiklund *et al.*,[17] etc.

Results of track-structure simulations rely on the accuracy of the cross sections for the various reaction channels of the considered particles. The light-ion transport codes RITRACKS, MC4, and PARTRAC use semiempirical ionization cross sections computed within different theoretical frameworks. RITRACKS is based on Rudd's semiempirical model whereas MC4 and PARTRAC cross sections are determined within the plane-wave Born approximation. However, the continuum distorted wave (CDW) method represents the state-of-the-art *ab initio* formalism for deriving the doubly differential cross sections (DDCSs) in the angle and energy of the ejected electron[18,19] pertaining to the ionization of atoms or molecules by ion impact. Since the theoretical expressions obtained within the CDW framework are very difficult to compute, simplifications are made to facilitate the numerical calculation of the DDCSs. To this category belongs the eikonal-initial-state approximation (CDW-EIS),[19–22] that has been recently incorporated in a few other MC codes[8,17,23,24] to describe the ionization of H_2O molecules by light ions. As for the inelastic interactions of electrons in condensed matter, the plane-wave Born approximation[25] with exchange and low-energy corrections constitutes the conventional framework to compute excitation and ionization cross sections from knowledge on the dielectric properties of the traversed medium. In this context, Dingfelder *et al.*[1,2] devised a parameterization of the dielectric response of water in the liquid phase, which is implemented, for instance, in PARTRAC, PITS04, and KITRACK.[26]

The aim of this paper is to present the newly developed MC tool LIonTrack (Light Ion Track) for the simulation of the spatial patterns of EDs by light ions in liquid water with physics models relevant for the nanometer scale. To optimize accuracy in this regime, the ionization by ion impact is described by the CDW-EIS cross sections. Furthermore, we transport the phase-space (initial energy, position, and direction) of the first-generation secondary electrons generated by LIonTrack with a modified version of PENELOPE/penEasy. PENELOPE is well adapted to deal with certain types of microdosimetry problems when operated in an event-by-event mode, as pointed out by several authors.[27–32] Nevertheless, when applying standard PENELOPE to track structure simulations, there are some limitations remaining due to the handling of inelastic interactions in condensed matter.[33] To remedy for this we utilize the aforementioned parameterization of the dielectric response of water in the liquid phase by Dingfelder *et al.*[1,2] With the novel approach of linking this model to PENELOPE/penEasy we achieve the degree of detail required for nanometer scales while retaining the advantages and capabilities of the standard PENELOPE code distributed by the OECD Nuclear Energy Agency. As a first application of LIonTrack, we present here the spatial patterns of EDs generated by single ion (proton, helium, lithium, and carbon) tracks. Specifically, we perform the clustering analysis in a novel way on the full spatial extension of the track and not in small selected volumes as previously presented by several authors.[15,34–38]

II. THE LIONTRACK MC CODE

The MC code consists of two separate packages. The first one transports light ions with specific energies E/M in the interval 1–300 MeV/u in liquid water. It utilizes precalculated tables of DDCSs from which the energy and emission angle of each secondary electron ejected by light-ion impact are sampled and stored in a "phase space file" along with the active molecular orbital and the position where the ionization took place (information on excitations is also scored). Additionally, this package also includes the Hansen–Kocbach–Stolterfoht (HKS) DDCS (Ref. 20) for 1–20 MeV/u protons that was adopted in our previous work.[39] The second package handles the transport of the secondary electrons, which are followed down to a selected absorption energy transport cutoff. Below such cutoff the remaining energy of the particle is deposited on the spot. This code is an *ad hoc* modification of the penEasy main program[40] that supplements the PENELOPE (version 2008) subroutine package[41] by replacing the default model for electron inelastic interactions in liquid water with tables of ionization and excitation cross sections computed from the formalism developed by Dingfelder *et al.*[1,2] Furthermore, a new tally has been added to penEasy to score the profile of EDs.

II.A. Cross sections for light ions

The ionization and excitation reaction channels for light ions with energy in the 1–300 MeV/u interval are included. Nuclear fragmentation is not considered. Furthermore, the light ions are assumed to follow straight trajectories, which is a good approximation for track-structure purposes where only a short longitudinal segment of the track is analyzed.

II.A.1. Ionization

The CDW-EIS formalism[19–22] is employed to calculate DDCSs, differential in the variables (energy ε_e and polar angle θ_e) of the ejected electron, as well as the corresponding singly differential cross sections (SDCSs) and total cross sections (TCSs). This model accounts for the postcollision Coulomb interaction of the outgoing electron with both the residual H_2O^+ ion (considered as a core with an effective charge) and the receding projectile. The ensuing two-center effects modify substantially the shape of the DDCS in the case of slow and/or highly charged light ions, yielding a conspicuous peak (the so-called "electron-capture to the continuum" peak) at forward angles when the velocity of the electron matches that of the ion. The present implementation of the CDW-EIS method expresses the initial wave function of each molecular orbital of the target H_2O molecule as a linear combination of Slater-type atomic orbitals with coefficients obtained from a population analysis.[24] In turn, the postcollision electron-target and electron-projectile interactions are represented through Coulomb fields where the effective charge of the target is determined from the experimental binding energy of the active molecular orbital in the liquid phase (or in the vapor phase when CDW-EIS cross sections are compared

with experiment). Finally, relativistic effects are incorporated in the kinematics of the projectile.

The methods developed to carry out the random sampling of ε_e and θ_e in ionizing collisions from the CDW-EIS cross-section tables are briefly outlined in the Appendix.

II.A.2. Excitation

A simple yet accurate way to obtain excitation cross sections for ions with $E/M \geq 1$ MeV/u relies on the scaling property (within the Born approximation) of cross sections with the projectile speed.[42] Then, excitation cross sections computed for relativistic electrons in liquid water[1,2] can be converted into the corresponding data for a light ion with the same speed by additionally scaling with the square of the projectile charge, again in the spirit of the first Born approximation.

II.B. Cross sections for electrons

II.B.1. Excitation, ionization, and atomic relaxation

The model implemented in PENELOPE to describe inelastic collisions of electrons is based on a schematic general oscillator strength for each atomic electron shell. This simple approach has several advantages. For instance, it can be employed to simulate the energy loss in arbitrary materials (elements, compounds, etc.) and performs well for quantities such as the mass collision stopping power. However, it oversimplifies the energy-loss SDCS for distant interactions, i.e., those which involve a small momentum transfer.[33] This is a drawback in certain microdosimetry applications as pointed out, e.g., by Bernal and Liendo.[32] To remedy for this limitation, we have adapted PENELOPE/penEasy so that, when an electron is being transported in liquid water, the default differential and total cross sections for inelastic interactions are replaced by those computed from the formalism set up by Dingfelder *et al.*[1,2] to describe both ionizations and excitations. In the case of ionization, the emission angle of the ejected electron is determined from the kinematics of a binary collision with a stationary electron. In what follows, PEN08 will refer to the default electron inelastic model in PENELOPE (version 2008) and DR08 will stand for Dingfelder *et al.*[1,2] cross sections.

When an ionization occurs in the oxygen K shell, either a KLL Auger electron or a Kα characteristic x-ray is released isotropically. Notice that, unlike in standard PENELOPE, we do not consider K-shell ionization of oxygen as an interaction mechanism that is decoupled from the energy-loss processes. In this way, artifacts that might show up in the form of negative energy imparted in very small scoring volumes are avoided.[33]

II.B.2. Elastic scattering and bremsstrahlung

The cross sections in PENELOPE for elastic scattering and bremsstrahlung interaction mechanisms (as well as for photon interactions) and the associated random sampling algorithms are kept unaltered. The elastic scattering database was obtained from relativistic partial-wave calculations carried out within the static-exchange approximation.[43,44] Cross sections calculated with this method have been published as ICRU Report 77 (Ref. 44) and as the "NIST Standard Reference Database 64" (NIST 2007). Moreover, similar approaches are currently behind some track-structure MC codes (see, e.g., Champion[45]). In turn, PENELOPE and most general-purpose codes rely on the SDCS database synthesized by Seltzer and Berger[46] to describe the energy-loss distribution of electron radiative losses. Furthermore, the polar emission angle of bremsstrahlung photons is sampled from Kissel *et al.*'s[47] partial-wave shape functions.

III. RESULTS AND DISCUSSION

III.A. Comparison of light-ion CDW-EIS cross sections with experimental data

We have undertaken an extensive comparison of existing experimental cross sections for the ionization of H_2O molecules, in the vapor phase, by light-ion impact with the predictions of the CDW-EIS formalism. For protons we compare to the DDCSs and SDCSs measured by Toburen and Wilson[48] and the SDCSs measured by Wilson *et al.*[49] In the case of alpha particles two experimental data sets have been reported in the literature, namely, the DDCSs of Toburen *et al.*[50] and the more recent measurements of DDCSs and SDCSs conducted by Ohsawa and co-workers.[51,52] In these experiments, the specific energies of the H^+ and He^{2+} ions spanned from 0.3 to 15 MeV/u. Ohsawa and co-workers[53] have also published experimental DDCSs and SDCSs for 6.0 MeV/u C^{6+} ions impinging on H_2O molecules. Apparently, there is lack of measurements above 15 MeV/u.

Although the amount of experimental information is limited, still the number of possible combinations of light ion, ion energy, and type of cross section is exceedingly large. However, we restrict ourselves to show just a few representative plots of DDCSs $d^2\sigma/d\varepsilon_e\, d\Omega_e$, SDCSs $d\sigma/d\varepsilon_e$, and TCSs σ. To avoid cluttering these graphs we do not display the uncertainty bars of the measured data, which in some cases may reach and even exceed 20%. The same reason motivated us not to include the predictions of other theoretical or semiempirical models. The interested reader may consult references[52–55] for comparisons of DDCSs, SDCSs, and TCSs computed within the first Born approximation or the HKS formalism and experimental values. For the sake of completeness, the electronic stopping power is briefly considered at the end of this subsection.

III.A.1. DDCSs

DDCSs for the impact of 1.5 MeV/u protons, 6.0 MeV/u alpha particles, and 6.0 MeV/u carbon ions on water vapor are displayed in Fig. 1. The CDW-EIS DDCSs are plotted as a function of $\cos\theta_e$ and compared to the experimental data of Toburen and Wilson,[48] Ohsawa *et al.*,[51] and Dal Cappello *et al.*[53] for several values of ε_e. For H^+ impact the agreement is quite good at intermediate angles, but at small and large angles the theoretical values fall below the measured

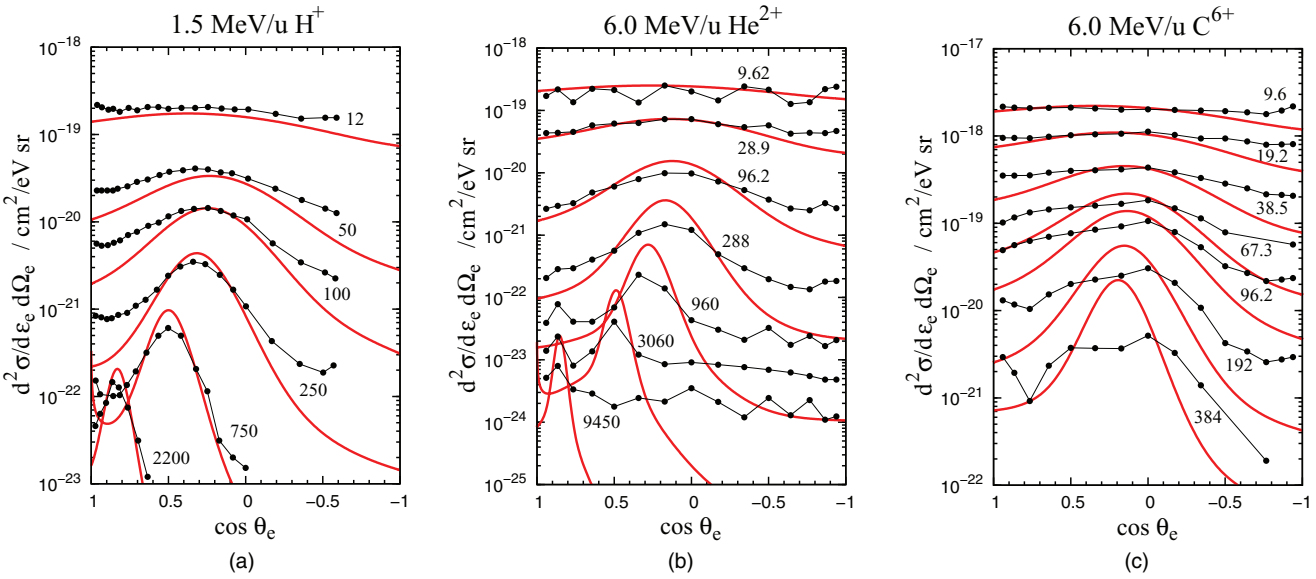

FIG. 1. DDCSs for the impact of 1.5 MeV/u H^+ (a), 6.0 MeV/u He^{2+} (b), and 6.0 MeV/u C^{6+} (c) ions on water vapor. The kinetic energies of the ejected electron are (top to bottom) 12, 50, 100, 250, 750, and 2200 eV (a); 9.62, 28.9, 96.2, 288, 960, 3060, and 9450 eV (b); and 9.6, 19.2, 38.5, 67.3, 96.2, 192, and 384 eV (c). The continuous curves are theoretical predictions of the CDW-EIS, whereas the symbols (joined by segments) correspond to measurements by Toburen and Wilson (Ref. 48) (a), Ohsawa *et al.* (Ref. 51) (b), and Dal Cappello *et al.* (Ref. 53) (c).

ones. In the case of He^{2+} and C^{6+} ions, the agreement is satisfactory for electrons ejected with $\varepsilon_e \lesssim 100$ eV, but deteriorates at higher energies. This is surprising because the experimental angular distribution is rather flat instead of developing the binary-encounter peak predicted by most theoretical approaches for an impulsive collision.[20] The overall accord is much better for 1.5 MeV/u H^+ ions, where a marked binary-encounter peak becomes visible in the experiment at ε_e above a few hundred eV. The discrepancies observed between the CDW-EIS results and the experimental data for electrons ejected with large energies at backward angles are a characteristic feature of the CDW-EIS model. In a recent publication[56] it has been described that, for atomic targets, the influence of the bound spectator electrons on the dynamic evolution of the ejected electron affects crucially the theoretical DDCSs (dynamic screening). The present CDW-EIS calculations take partially into account the dynamic screening through the effective target charge considered in the corresponding continuum factor of the exit channel. However, a residual perturbative potential associated with this interaction still remains. Fortunately, this shortcoming of the CDW-EIS model has a very limited influence on the simulation results reported below because large and very small emission angles have a relatively low probability of occurrence.

III.A.2. SDCSs

The energy distribution of the ejected electron is easier to measure than the DDCS; hence, the experimental uncertainties of the SDCSs are expected to be smaller except for $\varepsilon_e \lesssim 10$ eV. In fact, the large uncertainties in this part of the measured energy spectra preclude extracting definitive conclusions from the discrepancies between theory and experiment. Figure 2 depicts SDCSs corresponding to protons, alpha particles, and carbon ions with various energies. The predictions of the CDW-EIS formalism follow closely the experimental results of Wilson *et al.*[49] and Dal Cappello *et al.*[53] for H^+ and C^{6+} ions, respectively. However, the data of Ohsawa *et al.*[51] and Champion *et al.*[52] for He^{2+} ions show a strange curvature which is at variance with the anticipated ε_e^{-2} behavior (a straight line with slope equal to -2 on a log-log scale) when ε_e is much larger than the binding energy of the active molecular orbital but smaller than the maximum allowed energy transfer in a binary collision.[20] Ohsawa *et al.*[51] claim that a Fermi-shuttle acceleration mechanism (which is not modeled by the CDW-EIS) may be responsible for this shape of the SDCSs but the topic deserves further study. The peak observed in the experiments at $\varepsilon_e \approx 500$ eV originates from Auger electrons emitted after ionization of the oxygen K shell.

III.A.3. TCSs

TCSs for the ionization of H_2O molecules by the impact of protons, alpha particles, and carbon ions are shown in Fig. 3 as a function of the ion's specific energy. The CDW-EIS TCSs are compared to the measurements reported by Rudolph and Melton,[57] Bolorizadeh and Rudd,[58] Ohsawa *et al.*,[51] and Dal Cappello *et al.*[53] There is very good agreement between theory and experiment for H^+ and He^{2+}, especially for the latter, but the measured TCS of 6.0 MeV/u C^{6+} ions is considerably lower than the prediction of the CDW-EIS. The origin of this discrepancy remains to be understood.

III.A.4. Electronic stopping powers

The electronic stopping power S_e calculated from the CDW-EIS ionization cross sections, adding the contribution

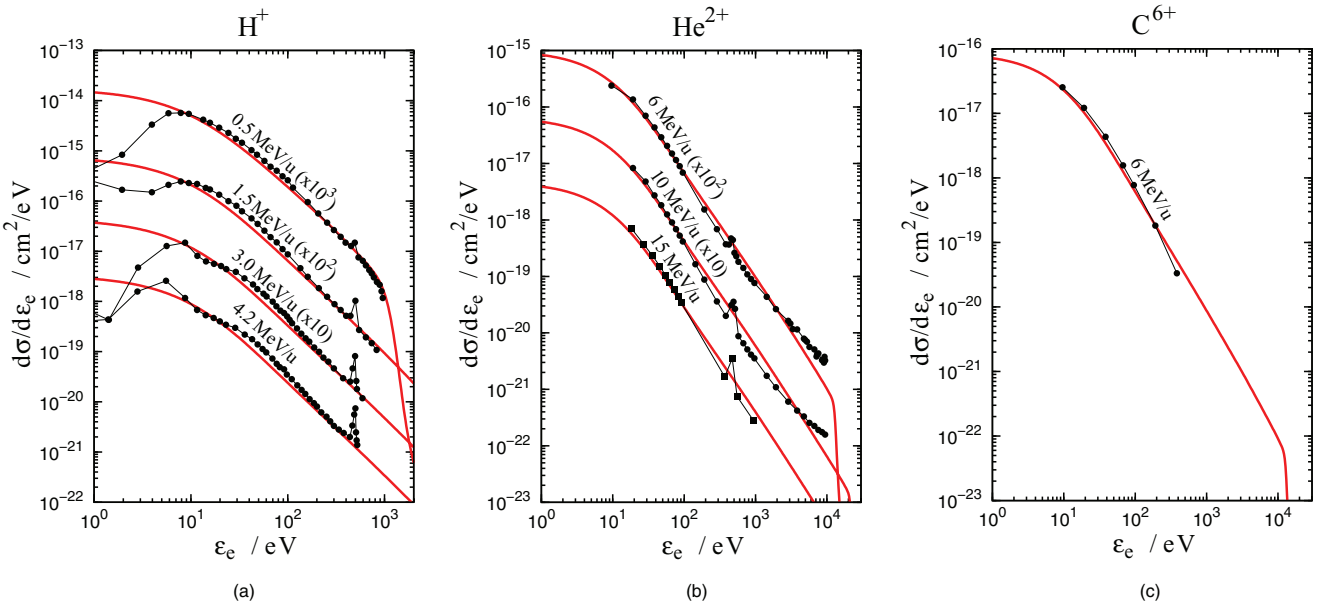

FIG. 2. SDCSs for the impact of H^+ (a), He^{2+} (b), and C^{6+} (c) ions on water vapor. The energies of the ion are (top to bottom) 0.5, 1.5, 3.0, and 4.2 MeV/u (a); 6.0, 10.0, and 15.0 MeV/u (b); and 6.0 MeV/u (c). The continuous curves are theoretical predictions of the CDW-EIS, whereas the symbols (joined by segments) correspond to measurements by Wilson *et al.* (Ref. 49) (a), Ohsawa *et al.* (Ref. 51) (circles) and Champion *et al.* (Ref. 52) (squares) (b), and Dal Cappello *et al.* (Ref. 53) (c). The data for 0.5, 1.5, and 3.0 MeV/u H^+ have been multiplied by 10^3, 10^2, and 10^1, respectively. The data for 6.0 and 10.0 MeV/u He^{2+} have been multiplied by 10^2 and 10^1, respectively.

due to excitation, was compared to the S_e tabulated in the ICRU Reports 49 for protons and alpha particles and 73 for heavier ions,[59,60] see Fig. 4. The contribution of excitation to S_e is about 2% for H^+, He^{2+}, Li^{3+}, and C^{6+} regardless of their specific energy. We recall that the calculated CDW-EIS cross sections pertain to bare ions, and thus only specific energies above 1 MeV/u are considered in order to avoid situations where charge-exchange effects (i.e., electron capture and loss by the ion) could be appreciable and render the comparison meaningless. Agreement is good, showing that the present set of cross sections is consistent with the ICRU recommendations. Small discrepancies are seen for C^{6+} and Li^{3+} ions below 1 MeV/u, most likely caused by the onset of charge exchange. This effect, which is accounted for in the data recommended by ICRU, tends to reduce the ion's effective charge and accordingly its electronic stopping power.

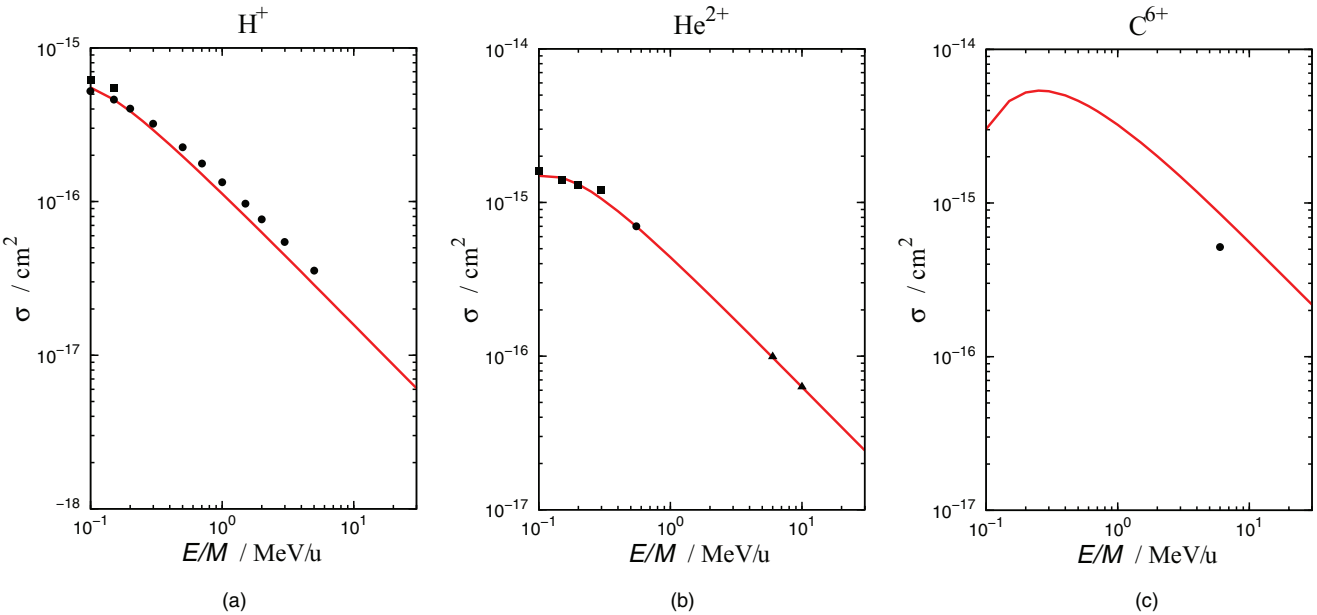

FIG. 3. TCSs of H^+ (a), He^{2+} (b), and C^{6+} (c) ions in water vapor as a function of the ion's specific energy. The continuous curves are theoretical predictions of the CDW-EIS, whereas the symbols correspond to measurements by Bolorizadeh and Rudd (Ref. 58) (a), Rudolph and Melton (Ref. 57) (circle) and Ohsawa *et al.* (Ref. 51) (squares) (b), and Dal Cappello *et al.* (Ref. 53) (c).

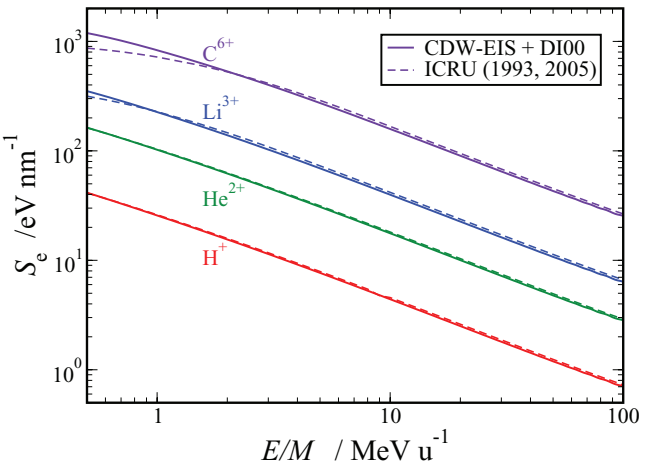

FIG. 4. Electronic stopping power of H^+, He^{2+}, Li^{3+}, and C^{6+} ions in liquid water as a function of the ions' specific energy. The continuous curves indicate the present cross sections, obtained by summing the contributions from ionization (CDW-EIS) and excitation (Ref. 42). The dashed curves are the recommendations of ICRU Reports 49 (Ref. 59) and 73 (Ref. 60), which pertain to ions that are partially dressed at low energies.

III.B. Applications to track-structure analysis

For the present study, we simulated ion track segments with lengths equal to three times the csda range of the most energetic secondary electron that may be emitted in an ionization. Only EDs in the middle csda range were postanalyzed to ensure longitudinal electronic equilibrium. In the first part of this section we present results for single ion tracks when varying the physics models of LIonTrack, for different energies and particle types. EDs from the full spatial extension of the track, along the middle csda range as explained above, were analyzed. The second part of this section regards radial dose distributions around the ion track and the energy deposited in nanometer-sized subvolumes around the track.

III.B.1. Spatial properties of EDs from single ion tracks

We have previously presented frequency distributions of distances between nearest-neighbor EDs only for proton track segments simulated with HKS ionization DDCSs.[39] The present investigation of the differences caused in such patterns by the use of other cross sections serves to quantify the sensitivity of the results coming from MC track-structure simulations in general. In this context, we have combined the CDW-EIS ion impact DDCSs with both the Dingfelder electron inelastic model (DR08) (the combination utilized in the LIonTrack code) and the default electron inelastic model in PENELOPE (PEN08) (the acronyms were defined in Subsection III.B.1) but also the previously used HKS ion impact DDCSs with both the DR08 and PEN08. The frequency distributions of nearest-neighbor distances d_1 for EDs generated with these combinations of cross sections are depicted in Fig. 5 for 1 and 10 MeV protons. The choice of either CDW-EIS or HKS DDCSs has only a small influence on the shape and the frequency yield of low-energy ions. This is to be expected as the electronic stopping power of both formalisms are in relatively good agreement and, in addition, the first Born approximation is adequate owing to the low atomic number of the projectile. In contrast, the frequency fall off from about 1 nm is much steeper when transporting the electrons with the default PENELOPE model instead of with the DR08 cross sections. By modeling the electron inelastic collisions in default PENELOPE with only three delta oscillators,[33] the average energy absorbed in a macro-

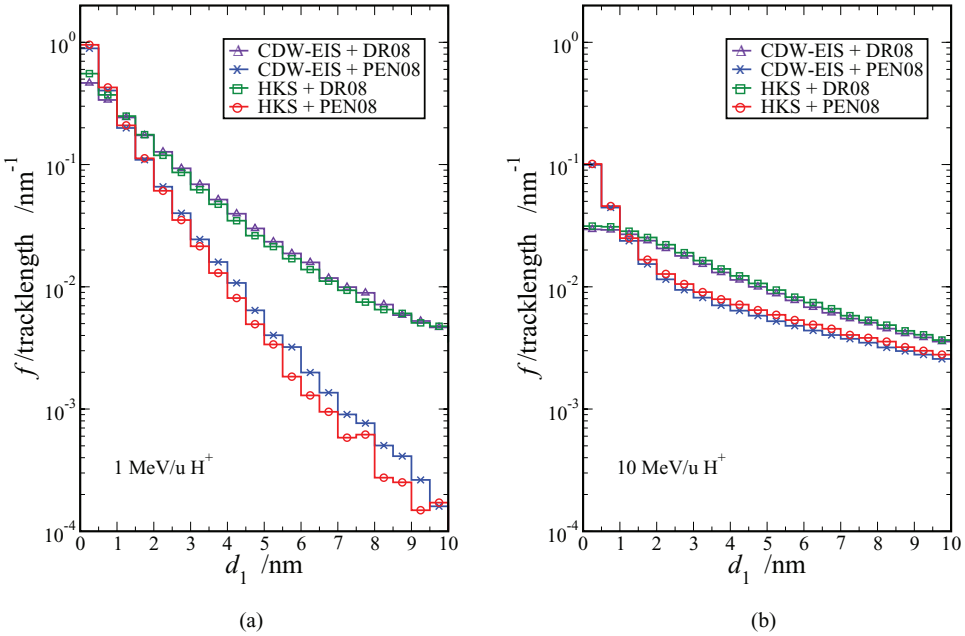

FIG. 5. Frequency distributions of first-nearest-neighbor ED distances, d_1, for 1 MeV/u (a) and 10 MeV/u (b) H^+ ions in liquid water. The four data sets were generated with the CDW-EIS + DR08 (triangles), CDW-EIS + PEN08 (crosses), HKS + DR08 (squares), and HKS + PEN08 (circles) cross sections.

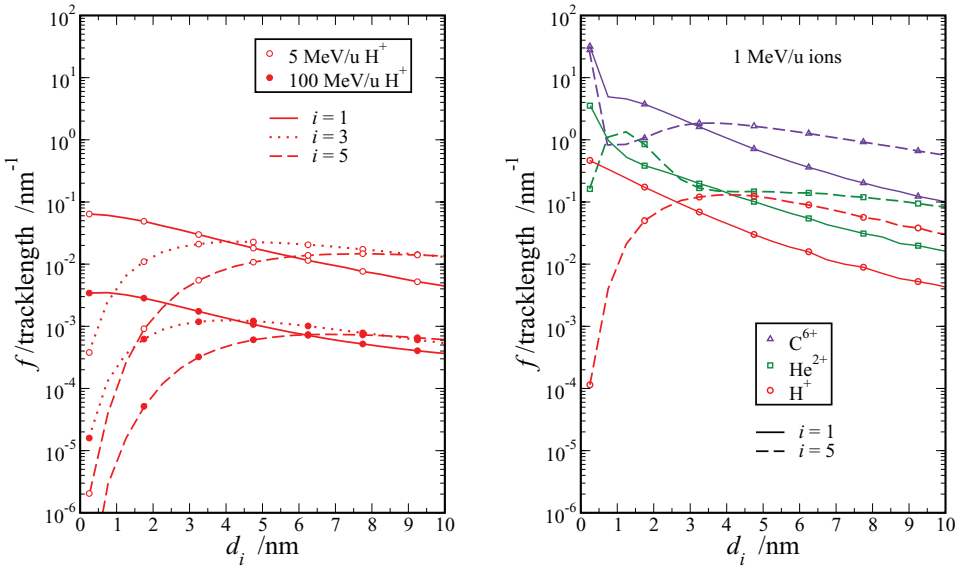

FIG. 6. Frequency distribution per unit length of ED distances d_i, with i equal to the neighbor order, to the first (continuous lines), third (dotted curves) [only panel (a)], and fifth (dashed lines) nearest ED by light ions in liquid water. Data in panel (a) display variation with the proton energy, 5 MeV/u (semifilled dots) and 100 MeV/u (filled dots). Analogous distributions are depicted for 1 MeV/u ions (open symbols): C^{6+} (triangles), He^{2+} (squares), and H^+ (circles) in panel (b). Data were generated with the CDW-EIS + DR08 cross sections.

scopic volume is conserved but the frequency of low-energy electrons is underestimated, ergo also the number of EDs. This oversimplification is blurred with increasing ion energy [Fig. 5(b)] due to the resulting increase of the energy and range of the ejected electrons.

Single ion tracks can be analyzed by looking into several aspects of the distributions of the frequency of distances d_i between EDs, such as the variation with the neighboring order i (e.g., with first, second, third, etc. nearest neighbors) and with the radiation quality. In that way the intrinsic clustering of EDs in single ion tracks can be quantified. Figure 6 displays the frequency distributions of distances to the first, third, and fifth neighbor for EDs when varying the particle energy [panel (a)] and to the first and fifth neighbor when varying the ion [panel (b)]. The frequency distributions of EDs are normalized per tracklength as they are analyzed for single ion tracks only. The frequency of all distances d_i between EDs decreases with increasing ion energy as expected as the ionization density decreases. Moreover, the higher the neighbor order i the lower the frequencies at small distances, which means that there are fewer clusters with many EDs within small distances. The frequency of distances to the closest neighbor d_1 is a decreasing function with increasing distances, while the frequencies for the higher neighbor orders increase with distance and show a broad maximum. The scores of nonclosest pairs become larger than the first nearest-neighbor at a certain distance which increases with neighbor order. For both 5 and 100 MeV/u protons, the crossing of the histograms for d_1 and d_3 takes place at around 4 nm, which is close to the distance between neighboring EDs of 3.4 nm suggested by various authors as to model an initial double strand break (dsb).[61] At about 3.4 nm, the C^{6+} ions produce about 23 times more pairs of nearest neighbors with the first ED mate than the H^+, but only about 15 times larger if the pair is formed by the fifth mate. It can be noted that the ratio of frequencies of EDs for a given specific energy of the projectile decreases with the neighbor order for up to 4 nm.

The mean distance $\bar{d}_i$ from one ED to its neighboring EDs provides a good description of the ED clustering in single ion tracks. In Table I the mean distances $\bar{d}_i$ to the first, second, third, fifth, and tenth neighbor ED for H^+, He^{2+}, Li^{3+}, and C^{6+} ions with specific energies equal to 1, 5, 20, and 50 MeV/u are listed. The mean distance increases with neighbor order and particle energy, and decreases with the projectile charge. In particular, if 3.4 nm is chosen as the distance between neighboring EDs to model an initial dsb, two to three EDs could be expected on average within that distance for 1 MeV/u H^+, and four to five EDs on average for 1 MeV/u C^{6+} ($\bar{d}_4 = 3.9$ nm).

III.B.2. Properties of energy absorption around single ion tracks

Radial dose distributions provide an insight into the spread of the energy deposited around the ion track. The absorbed dose as function of the radial distance ρ to the track center is depicted in Fig. 7 for 1 MeV/u protons (a) and 5 MeV/u ions (b). The histograms in panel (a) are results from MC codes with different cross sections and from the amorphous track model.[62] Specifically, the calculations by Wiklund *et al.*[17] resort to the CDW-EIS, like ours, but they transport the secondary electrons with the default models in PENELOPE-2006. Within the first 2 nm, the absorbed dose calculated with PENELOPE-2006 is higher but decreases faster than the radial dose obtained with DR08 (utilized in the LIonTrack code). This is consistent with the results of Fig. 5, where

TABLE I. Mean distance $\bar{d}_i$ (in nm) to the first, second, third, fifth, and tenth neighboring ED as a function of the radiation quality. Results are averaged over 1000 tracks.

	$\bar{d}_i$ (nm)				
E/*M* (MeV/u)	1	2	3	5	10
H^+					
1	2.2	4.0	5.5	8.4	14.7
5	5.5	10.2	14.6	22.7	40.5
20	12.1	22.3	31.5	48.0	84.0
50	20.5	37.3	52.2	79.7	141.7
He^{2+}					
1	1.8	3.0	4.1	6.0	9.9
5	4.2	7.6	10.7	16.2	27.7
20	8.4	15.0	20.5	29.7	46.7
50	12.6	21.6	28.8	40.5	64.0
Li^{3+}					
1	1.7	2.8	3.7	5.3	8.6
5	3.9	7.0	9.8	14.7	24.8
20	7.6	13.4	18.3	26.1	39.4
50	11.0	18.6	24.3	33.1	48.9
C^{6+}					
1	1.5	2.5	3.2	4.5	6.8
5	3.6	6.4	8.9	13.2	21.9
20	7.1	12.5	16.9	23.8	34.8
50	10.1	16.8	21.7	28.6	39.6

the PEN08 frequency distribution of d_1 decreases faster than that of DR08 beyond about 1.5 nm. Eventually the $D(\rho)$ histograms cross at $\rho \approx 3$ nm. From 0 to 0.1 nm the large absorbed dose is caused by the EDs in the track core, though the larger first radial bin employed by Emfietzoglou *et al.*[63] does not resolve this effect. In the interval 2–20 nm the three data sets give similar values. The radial dose distribution from the amorphous track model (that has been used to predict cell survival[62]) is proportional to, but overestimates, the results of the MC codes in the interval 20–50 nm. It is worth noting the $1/\rho$ dependence of the radial dose at short distances (below 2–3 nm), which means that the energy deposited per radial distance is rather constant in the vicinity of the track core (except for the peak due to the EDs by the ion itself). Another interesting feature is that the $D(\rho)$ histograms scale with the square of the projectile charge, indicating that effects beyond the plane-wave Born approximation included in the CDW-EIS cross sections have an imperceptible influence on the radial dose distributions of the considered light ions at (and above) 5 MeV/u.

Although the ion track core might not cross the DNA target, EDs by the secondary electrons can still occur at the DNA as the energy deposited in the DNA target depends on the ranges of these electrons (i.e., the radiation quality) and the proximity of the target to the track core. The mean energy imparted, $\langle\varepsilon\rangle$, to nanoscopic spherical targets as a function of the impact parameter b (the distance from the track to the center of the sphere) is presented in Fig. 8 for 1 MeV/u light ions. Data are plotted as $\langle\varepsilon\rangle/\phi$, where ϕ is the diameter of the sphere. $\langle\varepsilon\rangle/\phi$ decreases with b as the contribution of the track core diminishes. However, the contribution of EDs from the electron track-ends avoids a fall off to zero when the target is not at all crossed by the projectile, i.e., for $b > \phi/2$. Besides, the larger the sphere, the larger $\langle\varepsilon\rangle/\phi$ and the smoother the fall off. Moreover, $\langle\varepsilon\rangle/\phi$ increases with the ion's charge because of the enhanced LET. Values from LIonTrack are slightly lower than those reported by Emfietzoglou *et al.*[63] As one could anticipate, the most promi-

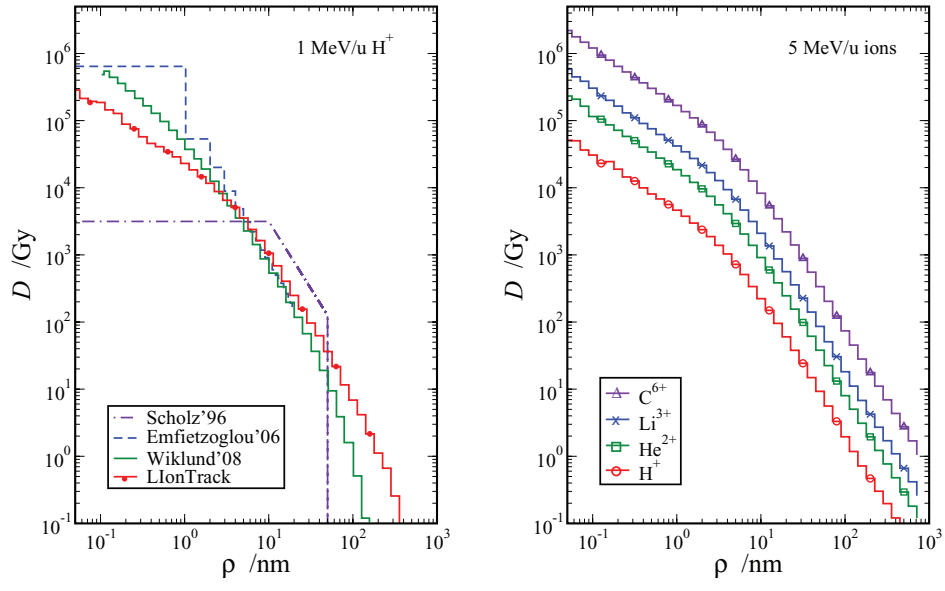

FIG. 7. Radial mean dose distributions for 1 MeV/u H^+ (a) and 5 MeV/u ions (b) in liquid water. The left panel corresponds to calculations for the present work (solid histogram with circles), Wiklund *et al.* (Ref. 17) (solid histogram), Emfietzoglou *et al.* (Ref. 63) (dashed histogram), and the amorphous track model [Scholz and Kraft (Ref. 62)] (dotted-dashed histogram). The right panel displays radial dose distributions for H^+ (circles), He^{2+} (squares), Li^{3+} (crosses), and C^{6+} ions (triangles) calculated with LIonTrack.

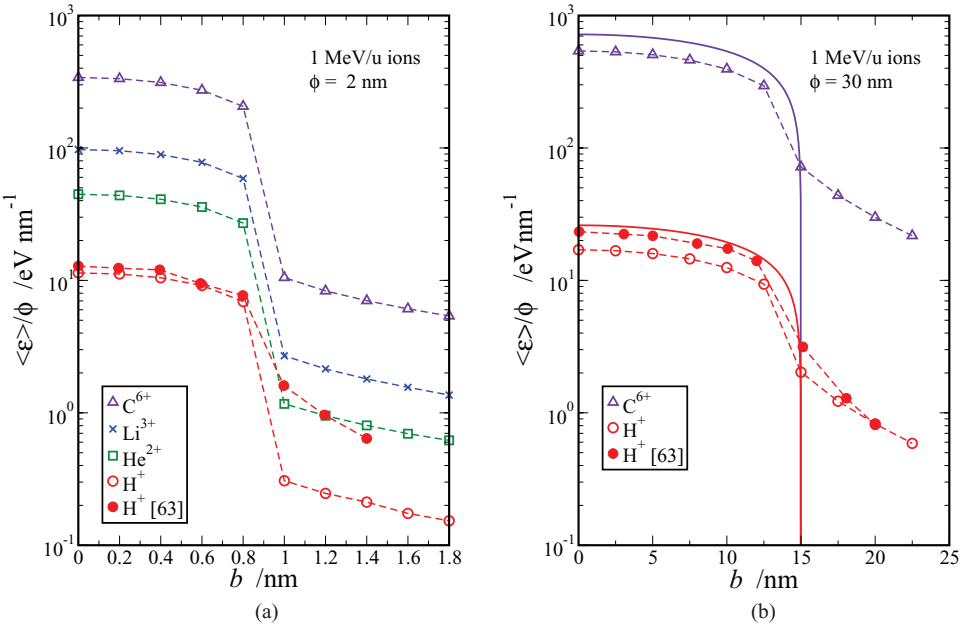

FIG. 8. Variation of the mean energy imparted with impact parameter for 1 MeV/u ion tracks traversing or passing near spheres of liquid water. The sphere diameters are $\phi = 2$ nm (a) and $\phi = 30$ nm (b). Calculations correspond to (top to bottom) C^{6+} (triangles), Li^{3+} (crosses), He^{2+} (squares), and H^+ (circles). The solid circles are data presented by Emfietzoglou *et al.* (Ref. 63) for 1 MeV/u H^+. Dashed lines are a guide for the eye. The solid curves in panel (b) are theoretical predictions based on the ICRU unrestricted LET of the ion and its path length inside the sphere. Data are plotted divided by the diameter of the sphere.

nent discrepancies appear outside the smallest of the considered spheres, where the stochastic nature of energy deposition is largest and the differences between the respective DDCSs become crucial. In the opposite limit of spheres with very large diameters $\langle\varepsilon\rangle/\phi$ should tend to the theoretical predictions obtained from the electronic stopping power (i.e., the unrestricted LET) multiplied by the ion path length inside the sphere, $l = 2\sqrt{(\phi/2)^2 - b^2}$; hence, the ratio $\langle\varepsilon\rangle_{b=0}/\phi$ should approach S_e. Interestingly, for the sphere with $\phi = 30$ nm we get $(\langle\varepsilon\rangle_{b=0}/\phi)/S_e \approx 2/3$, a ratio consistent with a rather uniform energy deposition at distances within about 15 nm from the ion's trajectory (see comment in connection with Fig. 7).

IV. CONCLUSIONS

The LIonTrack MC code presented here is suitable for the analysis of energy-deposition distributions by bare light ions in liquid water with reasonable accuracy in the nanometer scale. The package for the transport of secondary electrons, which links the Dingfelder *et al.*[1,2] model to PENELOPE/penEasy, was found to provide an accurate description of the excitations and ionizations that occur in liquid water while having the advantage of enabling both the use of PENELOPE's geometry package and the transport of electrons (and photons) in other materials.

The predictions of the CDW-EIS formalism employed to account for the ionization of H_2O molecules by light-ion impact have been compared to experimental data. Good agreement is found for most energies and angles of the ejected electrons, except for large energies in backward directions. The CDW-EIS model may be improved by including the dynamic screening in the final channel of the target.[64] This should result in better accord with the measurements both for backward and forward electron emissions.

The intrinsic EDs cluster capability by irradiation of a water medium by single ion tracks has been analyzed in a comprehensive form. For 1 MeV/u particles, C^{6+} ions generate about 15 times more clusters of six EDs within an ED distance of 3 nm than H^+. The probability of having larger clusters was found to decrease slowly with the size of the cluster.

The investigation herein should be extended from single track to multitrack analysis, as the intertrack effects are relevant in both experimental and clinical situations. Specifically, targets of the size of the cell nucleus are of concern as the EDs near the DNA structure can activate the pathways that prevent a cell from proliferating. Work along these lines is in progress.

ACKNOWLEDGMENTS

The authors are indebted to Dr. M. Dingfelder at East Carolina University for valuable discussions. Dr. D. Ohsawa at Kyoto University provided the authors with his experimental results in numerical form. Financial support from the Swedish Radiation Safety Authority (SSM) and the Swedish Research Council (VR) is gratefully acknowledged. J. M. Fernández-Varea acknowledges partial funding from the Spanish Ministerio de Ciencia e Innovación (Project No. FPA2009-14091-C02-01) and FEDER as well as the Generalitat de Catalunya (Project No. 2009 SGR 276). The computations were done on resources provided by SNIC through the Uppsala

Multidisciplinary Center for Advanced Computational Science (UPPMAX) under Project No. p2009001.

APPENDIX: RANDOM SAMPLING OF ε_e AND θ_e FROM TABLES OF SDCSs AND DDCSs FOR ION-IMPACT IONIZATION

The TCSs, SDCSs, and DDCSs describing the ionization of the five molecular orbitals of the H_2O molecule by light-ion impact are tabulated on a dense logarithmic grid of ion energies E_i. In turn, a logarithmic grid of 400 values of ε_e, ranging from 0.1 eV up to well above the energy of the binary-encounter peak, is used to tabulate the corresponding SDCSs and DDCSs. The latter are stored, for each ε_e, on a mesh of 91 angles $\theta_e = 0^\circ, 2^\circ, 4^\circ, \ldots, 180^\circ$.

In the course of the MC simulations the kinetic energy E of the light ion that is being transported will seldom coincide with one of the energies in the grid. Let us assume that $E_i \leq E \leq E_{i+1}$. Then, MC interpolation is performed to choose randomly either i or $i+1$ (see, e.g., Ref. 41). Afterward, the SDCS associated to the selected ion energy is used to sample ε_e by means of a rejection procedure. This procedure is implemented through a rejection function that takes advantage of the approximate shape $d\sigma/d\varepsilon_e \approx C\,\varepsilon_e^{-2}$ to achieve a reasonable efficiency of the algorithm (C is determined to yield the tightest possible upper bound of the SDCS). The sampled value of ε_e will not match any of the electron energies where the SDCS and its companion DDCS are tabulated. Therefore, a MC random interpolation is employed again to set from which one to do the subsequent sampling of θ_e (by the inverse-transform method).

The adopted grids and the coded sampling algorithms ensure that interpolation errors are kept well below 1%. Although the consumption of random-access memory is substantial, nowadays this is not an issue.

[a]Electronic mail: jose@ecm.ub.edu

[1]M. Dingfelder, D. Hantke, M. Inokuti, and H. G. Paretzke, "Electron inelastic-scattering cross sections in liquid water," Radiat. Phys. Chem. **53**, 1–18 (1998).
[2]M. Dingfelder, R. H. Ritchie, J. E. Turner, W. Friedland, H. G. Paretzke, and R. N. Hamm, "Comparisons of calculations with PARTRAC and NOREC: Transport of electrons in liquid water," Radiat. Res. **169**, 584–594 (2008).
[3]International Commission on Radiation Units and Measurements, "Fundamental quantities and units for ionizing radiation," ICRU Report 60 (ICRU Publications, Bethesda, 1998).
[4]D. T. Goodhead, "Energy deposition stochastics and track structure: What about the target?" Radiat. Prot. Dosim. **122**, 3–15 (2006).
[5]B. Grosswendt, "Nanodosimetry, the metrological tool for connecting radiation physics with radiation biology," Radiat. Prot. Dosim. **122**, 404–414 (2006).
[6]A. Ottolenghi, M. Merzagora, and H. G. Paretzke, "DNA complex lesions induced by protons and α-particles: Track structure characteristics determining linear energy transfer and particle type dependence," Radiat. Environ. Biophys. **36**, 97–103 (1997).
[7]D. Emfietzoglou, K. Karava, G. Papamichael, and M. Moscovitch, "Monte Carlo simulation of the energy loss of low-energy electrons in liquid water," Phys. Med. Biol. **48**, 2355–2371 (2003).
[8]C. Champion, A. L'Hoir, M. F. Politis, P. D. Fainstein, R. D. Rivarola, and A. Chetioui, "A Monte Carlo code for the simulation of heavy-ion tracks in water," Radiat. Res. **163**, 222–231 (2005).
[9]C. Champion and C. L. Loirec, "Positron follow-up in liquid water: I. A new Monte Carlo track-structure code," Phys. Med. Biol. **51**, 1707–1723 (2006).
[10]H. Nikjoo, S. Uehara, D. Emfietzoglou, and F. A. Cucinotta, "Track-structure codes in radiation research," Radiat. Meas. **41**, 1052–1074 (2006).
[11]M. Zaider, D. J. Brenner, and W. E. Wilson, "The applications of track calculations to radiobiology. 1. Monte Carlo simulation of proton tracks," Radiat. Res. **95**, 231–247 (1983).
[12]S. Uehara, H. Nikjoo, and D. T. Goodhead, "Cross-sections for water vapour for the Monte Carlo electron track structure code from 10 eV to the MeV region," Phys. Med. Biol. **38**, 1841–1858 (1993).
[13]V. A. Semenenko, J. E. Turner, and T. B. Borak, "NOREC, a Monte Carlo code for simulating electron tracks in liquid water," Radiat. Environ. Biophys. **42**, 213–217 (2003).
[14]W. E. Wilson, J. H. Miller, D. J. Lynch, R. R. Lewis, and M. Batdorf, "Analysis of low-energy electron track structure in liquid water," Radiat. Res. **161**, 591–596 (2004).
[15]W. Friedland, M. Dingfelder, P. Jacob, and H. G. Paretzke, "Calculated DNA double-strand break and fragmentation yields after irradiation with He ions," Radiat. Phys. Chem. **72**, 279–286 (2005).
[16]I. Plante and F. A. Cucinotta, "Ionizations and excitation cross sections for the interaction of HZE particles in liquid water and application to Monte Carlo simulation of radiation tracks," New J. Phys. **10**, 125020 (2008).
[17]K. Wiklund, G. H. Olivera, A. Brahme, and B. K. Lind, "Radial secondary electron dose profiles and biological effects in light-ion beams based on analytical and Monte Carlo calculations using distorted wave cross sections," Radiat. Res. **170**, 83–92 (2008).
[18]C. Champion, O. Boudrioua, and C. D. Cappello, "Water molecule ionization by charged particles: A short review," J. Phys.: Conf. Ser. **101**, 012010 (2008).
[19]D. Belkić, "Review of theories on ionization in fast ion-atom collisions with prospects for applications to hadron therapy," J. Math. Chem. **47**, 1366–1419 (2010).
[20]N. Stolterfoht, R. D. DuBois, and R. D. Rivarola, *Electron Emission in Heavy Ion-Atom Collisions* (Springer, Berlin, 1997).
[21]M. E. Galassi, R. D. Rivarola, M. Beuve, G. H. Olivera, and P. D. Fainstein, "Theoretical calculation of single ionisation in collisions between protons and low-Z molecules at intermediate and high energies," Phys. Rev. A **62**, 022701 (2000).
[22]R. D. Rivarola, M. E. Galassi, P. D. Fainstein, and C. Champion, "Computation of distorted wave cross sections for high-energy inelastic collisions of heavy ions with water molecules," Adv. Quantum Chem. **65**, 231–267 (2013).
[23]B. Gervais, M. Beuve, G. H. Olivera, M. E. Galassi, and R. D. Rivarola, "Production of HO_2 and O_2 by multiple ionization in water radiolysis by swift carbon ions," Chem. Phys. Lett. **410**, 330–334 (2005).
[24]B. Gervais, M. Beuve, G. H. Olivera, and M. E. Galassi, "Numerical simulation of multiple ionization and high LET effects in liquid water radiolysis," Radiat. Phys. Chem. **75**, 493–513 (2006).
[25]M. Inokuti, "Inelastic collisions of fast charged particles with atoms and molecules—The Bethe theory revisited," Rev. Mod. Phys. **43**, 297–347 (1971).
[26]K. Wiklund, J. M. Fernández-Varea, and B. K. Lind, "A Monte Carlo program for the analysis of low-energy electron tracks in liquid water," Phys. Med. Biol. **56**, 1985–2003 (2011).
[27]R. D. Stewart, W. E. Wilson, J. C. McDonald, and D. J. Strom, "Microdosimetric properties of ionizing electrons in water: A test of the PENELOPE code system," Phys. Med. Biol. **47**, 79–88 (2002).
[28]E. Mainardi, R. J. Donahue, W. E. Wilson, and E. A. Blakely, "Comparison of microdosimetric simulations using PENELOPE and PITS for a 25 keV electron microbeam in water," Radiat. Res. **162**, 326–331 (2004).
[29]R. P. Hugtenburg, Z. Chaoui, and J. E. Pattison, "Microdosimetric event distributions in sub-cellular volumes with a general purpose Monte Carlo code," Nucl. Instrum. Methods Phys. Res. A **580**, 157–160 (2007).
[30]Y. Hsiao and R. D. Stewart, "Monte Carlo simulation of DNA damage induction by x-rays and selected radioisotopes," Phys. Med. Biol. **53**, 233–244 (2008).
[31]R. P. Hugtenburg, "Microdosimetry in X-ray synchroton based binary radiation therapy," Eur. J. Radiol. **68S**, S126–S128 (2008).
[32]M. A. Bernal and J. A. Liendo, "An investigation on the capabilities of the PENELOPE MC code in nanodosimetry," Med. Phys. **36**, 620–625 (2009).
[33]J. M. Fernández-Varea, G. González-Muñoz, M. E. Galassi, K. Wiklund, B. K. Lind, A. Ahnesjö, and N. Tilly, "Limitations (and merits)

of PENELOPE as a track-structure code," Int. J. Radiat. Biol. **88**, 66–70 (2012).
[34]D. T. Goodhead, H. P. Leenhouts, H. G. Paretzke, M. Terrissol, H. Nikjoo, and R. Blaauboer, "Track structure approaches to the interpretation of radiation effects on DNA," Radiat. Prot. Dosim. **52**, 217–223 (1994).
[35]V. Michalik, "Distance distributions for energy deposition clusters in different particle tracks," Radiat. Prot. Dosim. **52**, 245–248 (1994).
[36]A. Ottolenghi, M. Merzagora, L. Tallone, M. Durante, H. G. Paretzke, and W. E. Wilson, "The quality of DNA double-strand breaks: A Monte Carlo simulation of the end-structure of strand breaks produced by protons and alpha particles," Radiat. Environ. Biophys. **34**, 239–444 (1995).
[37]F. A. Cucinotta, H. Nikjoo, and D. T. Goodhead, "Model for radial dependence of frequency distributions for energy imparted in nanometer volumes from HZE particles," Radiat. Res. **153**, 459–468 (2000).
[38]H. Nikjoo, D. Emfietzoglou, R. Watanabe, and S. Uehara, "Can Monte Carlo track structure codes reveal reaction mechanism in DNA damage and improve radiation therapy?" Radiat. Phys. Chem. **77**, 1270–1279 (2008).
[39]G. González-Muñoz, N. Tilly, J. M. Fernández-Varea, and A. Ahnesjö, "Monte Carlo simulation and analysis of proton energy-deposition patterns in the Bragg peak," Phys. Med. Biol. **53**, 2857–2875 (2008).
[40]J. Sempau, A. Badal, and L. Brualla, "A PENELOPE-based system for the automated Monte Carlo simulation of clinacs and voxelized geometries—Application to far-from-axis fields," Med. Phys. **38**, 5887–5895 (2011).
[41]F. Salvat, J. M. Fernández-Varea, and J. Sempau, *PENELOPE-2008: A Code System for Monte Carlo simulation of Electron and Photon Transport* (OECD Nuclear Energy Agency, Issy-les-Moulineaux, 2008).
[42]M. Dingfelder, M. Inokuti, and H. G. Paretzke, "Inelastic-collision cross sections of liquid water for interactions of energetic protons," Radiat. Phys. Chem. **59**, 255–275 (2000).
[43]F. Salvat, A. Jablonski, and C. J. Powell, "ELSEPA—Dirac partial-wave calculation of elastic scattering of electrons and positrons by atoms, positive ions and molecules," Comput. Phys. Commun. **165**, 157–190 (2005).
[44]International Commission on Radiation Units and Measurements, "Elastic scattering of electrons and positrons," ICRU Report 77 (ICRU Publications, Bethesda, 2007).
[45]C. Champion, "Theoretical cross sections for electron collisions in water: Structure of electron tracks," Phys. Med. Biol. **48**, 2147–2168 (2003).
[46]S. M. Seltzer and M. J. Berger, "Bremsstrahlung energy spectra from electrons with kinetic energy 1 keV-10 GeV incident on screened nuclei and orbital electrons of neutral atoms with $Z = 1 - 100$," At. Data Nucl. Data Tables **35**, 345–418 (1986).
[47]L. Kissel, C. A. Quarles, and R. H. Pratt, "Shape functions for atomic-field bremmstrahlung from electrons of kinetic energy 1-500 keV on selected neutral atoms $1 \leq Z \leq 92$," At. Data Nucl. Data Tables **28**, 381–460 (1983).
[48]L. H. Toburen and W. E. Wilson, "Energy and angular distributions of electrons ejected from water vapor by 0.3-1.5 MeV protons," J. Chem. Phys. **66**, 5202–5213 (1977).
[49]W. E. Wilson, J. H. Miller, and L. H. Toburen, "Differential cross sections for ionization of methane, ammonia, and water vapor by high velocity ions," J. Chem. Phys. **80**, 5631–5638 (1984).
[50]L. H. Toburen, W. E. Wilson, and R. J. Popowich, "Secondary electron emission from ionization of water vapor by 0.3- to 2.0-MeV He^+ and He^{2+} ions," Radiat. Res. **82**, 27–44 (1980).
[51]D. Ohsawa, Y. Sato, Y. Okada, V. P. Shevelko, and F. Soga, "6.0-10.0-MeV/u He^{2+}-ion-induced electron emission from water vapor," Phys. Rev. A **72**, 062710 (2005).
[52]C. Champion, O. Boudrioua, C. D. Capello, Y. Satov, and D. Ohsawa, "Theoretical and experimental investigations of electron emission in $He^{2+}+H_2O$ collisions," Phys. Rev. A **75**, 032724 (2007).
[53]C. D. Cappello, C. Champion, O. Boudrioua, H. Lekadir, Y. Sato, and D. Ohsawa, "Theoretical and experimental investigations of electron emission in $C^{6+}+ H_2O$ collisions," Nucl. Instrum. Methods Phys. Res. B **267**, 781–790 (2009).
[54]C. Champion and C. D. Cappello, "Theoretical investigations of electron emission after water vapour ionization by light ion impact," Nucl. Instrum. Methods Phys. Res. B **267**, 881–884 (2009).
[55]M. A. Bernal-Rodríguez and J. A. Liendo, "Single ionization of liquid water by protons, alpha particles, and carbon nuclei: Comparative analysis of the continuum distorted wave methodologies and empirical models," Adv. Quantum Chem. **65**, 203–229 (2013).
[56]J. M. Monti, O. A. Fojón, J. Hanssen, and R. D. Rivarola, "Influence of the dynamic screening on single-electron ionization of multi-electron atoms," J. Phys. B: At. Mol. Opt. Phys. **43**, 205203 (2010).
[57]P. S. Rudolph and C. E. Melton, "Experimental and theoretical considerations for ionization of simple hydrocarbons, H_2, D_2, O_2, H_2O, and the rare gases by 2.2-MeV α particles and by electrons in a mass spectrometer," J. Chem. Phys. **45**, 2227–2232 (1966).
[58]M. A. Bolorizadeh and M. E. Rudd, "Angular and energy dependence of cross sections for ejection of electrons from water vapor. II. 15–150-keV proton impact," Phys. Rev. A **33**, 888–892 (1986).
[59]ICRU International Commission on Radiation Units and Measurements, "Stopping powers and ranges for protons and alpha particles," ICRU Report 49 (ICRU Publications, Bethesda, 1993).
[60]International Commission on Radiation Units and Measurements, "Stopping of ions heavier than helium," ICRU Report 73 (ICRU Publications, Bethesda, 2005).
[61]H. Nikjoo, P. O'Neill, M. Terrissol, and D. T. Goodhead, "Quantitative modelling of DNA damage using Monte Carlo track structure method," Radiat. Environ. Biophys. **38**, 31–38 (1999).
[62]M. Scholz and G. Kraft, "Track structure and the calculation of biological effects of heavy charged particles," Adv. Space Res. **18**, 5–14 (1996).
[63]D. Emfietzoglou, H. Nikjoo, G. Papamichael, and A. Pathak, "Proton beam profiling in soft biological matter by detailed Monte Carlo simulation," Nucl. Instrum. Methods Phys. Res. B **249**, 670–672 (2006).
[64]J. M. Monti, C. A. Tachino, J. Hanssen, O. A. Fojón, M. E. Galassi, C. Champion, and R. D. Rivarola, "Distorted wave calculations for electron loss process induced by bare ion impact on biological targets," Appl. Radiat. Isotopes (2013) (in press).